

---

## Automated Short Distance Vehicle Following Using a Dynamic Base RTK System

---

William Travis,\* Scott Martin, and David M. Bevly

The GPS and Vehicle Dynamics Lab  
Auburn University  
270 Ross Hall  
Mechanical Engineering  
Auburn, AL 36849  
Email: [traviwe@auburn.edu](mailto:traviwe@auburn.edu)  
Email: [smm0008@auburn.edu](mailto:smm0008@auburn.edu)  
Email: [bevlydm@auburn.edu](mailto:bevlydm@auburn.edu)  
\*Corresponding Author

**Abstract:** Real time results from a close distance vehicle platoon in which the lead vehicle was man driven and the following vehicle was automated are shown. A Dynamic base RTK (DRTK) algorithm was used to determine a precise relative position vector between the vehicles. The vector was used as a means of controlling the following vehicle to the lead vehicle's path of travel. The DRTK algorithm, control concept, and automated convoy are described. Results show the accuracy of the DRTK algorithm to be centimeter level and demonstrate the feasibility of the control concept. The standard deviation of path tracking error when driving straight was 0.24 m. Error while turning is a function of turning radius and baseline length. An expression for the theoretical error is provided, and error from real time tests is shown for different separation distances.

**Keywords:** unmanned ground vehicle; UGV; autonomous; relative position; RTK; GPS; GNSS; convoy; platoon.

**Reference** to this paper should be made as follows: Travis, W., Martin, S., and Bevly, D.M. (20##) 'Automated short distance vehicle following using a dynamic base RTK system', *Int. J. Vehicle Autonomous Systems*, Vol. #, Nos. #, pp. #-#.

**Biographical notes:** William Travis is a graduate student in the GPS and Vehicle Dynamics Lab at Auburn University in Auburn, Alabama studying ground vehicle navigation. He graduated with a B.S. in Mechanical Engineering in 2004 and a M.S. in Mechanical Engineering in

*Author*

2006, both from Auburn University. Currently research is investigating relative positioning strategies for ground vehicles. Areas of experience include guidance and navigation systems, GPS, ground vehicle dynamics, and control systems.

Scott Martin graduated with a B.S in Engineering, from East Carolina University. He is currently a Mechanical Engineering pursuing a Master's degree and a research assistant in the GPS and Vehicle Dynamics Laboratory at Auburn University. His research interests include GPS, automation and control, and navigation.

David M. Bevly received his B.S. from Texas A&M University, an M.S. from Massachusetts Institute of Technology, and a Ph.D. from Stanford University in mechanical engineering. Bevly directs Auburn University's GPS and Vehicle Dynamics Laboratory (GAVLAB), which focuses on modeling, navigation, and control of vehicles.

## **1. Introduction**

Ground vehicles traveling in a close convoy or platoon, where one or more vehicles, potentially of varying types, follow a lead vehicle, experience an increase in safety and energy efficiency while decreasing congestion on road ways. Replacing the driver with a control system can enhance the benefits gained by platooning. Safety can be improved by reducing driver fatigue over long operation periods, mitigating effects due to driver error, and by controlling the vehicle with more precision and consistency than the average driver. Efficiency improvements are gained because the vehicles can maintain optimal convoy formations to maximize fuel economy consistently and operate for longer periods of time than a man driven vehicle. Also, less focus is required to operate the vehicle, so the driver is freed to perform other tasks.

An automated ground vehicle convoy could affect both civilian and military operations. The military would notice an immediate impact in areas of logistics and surveillance as transportation of supplies would require a smaller number of soldiers, and drivers could place a larger portion of their focus on the surrounding environment rather than on vehicle operation. A civilian transportation company could use a small number of drivers to transport a fleet of vehicles. It could also employ a continuous operation strategy where drivers of the lead vehicle change periodically to keep the convoy moving, which would safely bypass legal restrictions on driving time by professional drivers without actually adding

*Title*

more drivers. Agricultural efforts of planting and harvesting require precise vehicle formations and cooperation to minimize waste and operation time, thereby maximizing output and profit.

The concept of an automated vehicle convoy is not new; it can be traced back to the 1939 World's Fair (Tomizuka, 1994). However, approaches to the problem have changed as new technology becomes available. Much work was done in the area in the mid 1980s to 1990s by the California PATH (Partners for Advanced Transit and Highways) program. Magnets were embedded into public roadways, and magnetometers on each vehicle provided the vehicle with knowledge of its position in the lane. Other work utilizes perception sensors so vehicles can literally see one another. Recognizable objects are placed on the back of the lead vehicle, and a laser scanner (Chen et al., 2004) or camera can be used to determine relative position and orientation from the following to lead vehicle.

Carrier phase differential GPS can be used to provide a reference in which an automated vehicle can trail a lead vehicle. This technique was chosen in this work because a standalone GPS solution is inadequate for inter-vehicle positioning (Kellum, 2005). Specifically, a Dynamic base RTK (DRTK) algorithm is used to determine high accuracy relative position and orientation between vehicles. Similar algorithms are used for formation flight (Felter and Wu, 1997), automated aircraft refueling (Khanafseh, Kempny, and Pervan, 2006), automated shipboard landings (Dogra, Wright, and Hansen, 2005), and to measure ship flexure (Petovello, Lachapelle, and Cannon, 2005). This approach is not constrained by the necessity of additional infrastructure in the operational environment, and it can work in scenarios where perception systems are unreliable because line-of-sight (LOS) between vehicles cannot be established. Also, simulation has shown the capability for non-line-of-sight (NLOS) operation (Travis and Bevely, 2008). The deficiencies of this method are that the vehicles must maintain lock onto a common set of GPS satellites, which can be difficult in some environments. Other sensors, such as a laser scanner, camera, or inertial system, could be incorporated to improve its robustness and overcome some shortcomings.

A method is presented in this work that enables an unmanned ground vehicle (UGV) to follow a human driven lead vehicle. A DRTK solution is used to formulate the control reference with the goal of replicating the lead vehicle's path of travel when following at a short distance. Real time performance of the DRTK algorithm and the vehicle following system are shown. Section 2 gives a brief overview of the DRTK algorithm and its real time accuracy. The UGV steering control

*Author*

and its local onboard navigation system is presented in Section 3. Section 0 discusses the experimental set up, and Section 5 shows the real time results of the implemented method, including lateral path error. Section 6 concludes with a short discussion of the results.

## 2. DRTK

The DRTK algorithm is similar in concept to a Real Time Kinematic (RTK) algorithm, where spatially and temporally correlated measurement errors are removed by the differencing of computed range measurements from multiple receivers. An RTK system uses a receiver at a known, static location in conjunction with a receiver on a moving platform to determine a precise global position of the platform, where typical errors are on the order of centimeters. A DRTK system computes a very precise relative position between antennas on moving platforms. The constraint of the static base station is removed at the expense of the availability of a precise global position solution.

### 2.1. Algorithm Description

The carrier phase measurement is utilized to achieve the most accurate solution. Code phase measurements are unambiguous, but ranging errors are around half a meter. Carrier phase measurements can be used to form millimeter accurate range information, but they suffer from an unknown cycle ambiguity. The cycle ambiguity is the integer number of cycles of the carrier signal between the antenna and a GPS satellite when the receiver locks on to the signal. Therefore, the ambiguities must be determined in order to produce the most accurate relative position solution.

Consider code and phase based range measurements ( $\rho$  and  $\phi$ ) from a receiver at location  $A$  to satellite  $j$  (Misra and Enge, 2006).

$$\rho_A^j = |\vec{r}_A^j| + c(\delta t_A - \delta t^j) + \lambda(T^j + I^j) + \epsilon_\rho^j \quad (1)$$

$$\phi_A^j = |\vec{r}_A^j| + c(\delta t_A - \delta t^j) + \lambda(T^j - I^j + N^j) + \epsilon_\phi^j \quad (2)$$

The measurements are in units of distance. Unknowns in the measurement consist of a true range magnitude ( $|\vec{r}_A^j|$ ), a receiver clock bias ( $\delta t_A$ ), a satellite clock bias ( $\delta t^j$ ), a tropospheric error ( $T$ ), ionospheric error ( $I$ ), the integer cycle ambiguity ( $N$ ), and measurement noise including multipath ( $\epsilon$ ). Note that multipath errors on the carrier measurement are two orders of magnitude smaller than on the code measurement (Hofmann-

*Title*

Wellenhof, Lichtenegger, and Collins, 2001). The known variables are the speed of light ( $c$ ) and the carrier wavelength ( $\lambda$ ). Determining the ambiguities is not possible over short measurement periods due to the number and magnitude of other unknowns. However, the measurement errors are correlated among receivers in close proximity (<20km).

Differencing time synchronized measurements from a receiver at location  $B$  from those the receiver at location  $A$  produces single differenced measurements (denoted by  $\Delta$ ), where the ranges are between antennas at  $A$  and  $B$  instead of between an antenna and a GPS satellite.

$$\Delta\rho_{AB}^j = |\Delta\vec{r}_{AB}^j| + c\delta t_{AB} + \epsilon_{\Delta\rho}^j \quad (3)$$

$$\Delta\phi_{AB}^j = |\Delta\vec{r}_{AB}^j| + c\delta t_{AB} + \lambda\Delta N^j + \epsilon_{\Delta\phi}^j \quad (4)$$

The atmospheric errors and satellite clock bias errors are mitigated. The remaining terms are a relative range between  $A$  and  $B$ , error due to the receivers' clocks, a single differenced ambiguity, and noise. The single differenced noise increases over the un-differenced noise by an approximate factor of  $\sqrt{2}$  due to the combination of measurements. Placing  $2m$  single differenced code and carrier range measurements in matrix form, where  $m$  is the number of visible satellites, yields the following:

$$\begin{bmatrix} \Delta\rho \\ \Delta\phi \end{bmatrix}_{2m \times 1} = \bar{G}_{2m \times 4} \begin{bmatrix} \Delta\vec{r}_{AB} \\ c\delta t_{AB} \end{bmatrix}_{4 \times 1} + \begin{bmatrix} 0_{m \times m} \\ \lambda I_{m \times m} \end{bmatrix} \Delta N_{m \times 1} \quad (5)$$

where

$$\bar{G} = \begin{bmatrix} G & 1 \\ G & 1 \end{bmatrix} \quad (6)$$

and  $G$  is an  $m \times 3$  matrix known as the geometry matrix containing the three dimensional unit vectors from location  $A$  to each satellite.

At this point, the relative position and clock terms are nuisance parameters and do need not to be determined. The left null space of  $\bar{G}$  is defined such that

$$L\bar{G} = 0 \quad (7)$$

Equation (5) can be rewritten with the nuisance terms removed.

Author

$$L \begin{bmatrix} \Delta\rho \\ \Delta\phi \end{bmatrix} = L \begin{bmatrix} 0 \\ \lambda I \end{bmatrix} \Delta N \quad (8)$$

Alternatively, a more compact notation can be used:

$$z_k = H_k \hat{x}_k \quad (9)$$

where the measurement vector and matrix are denoted by  $z$  and  $H$ , respectively, at time  $k$ .

The measurement covariance is a function of the single differenced measurement variances and the left null space. The un-differenced measurement noise can be approximated by determining the accuracy of the delay and phase lock loops in the receiver. Standard formulas for the tracking loop accuracy are given in (Misra and Enge, 2006) and (Kaplan and Hegarty, 2006). Under the assumption that the ionospheric and satellite clock errors were removed, the single differenced measurement error variance can be calculated by summing the tracking loop error variances from each receiver. The single differenced measurement covariance can be expressed as follows:

$$\bar{R} = \begin{bmatrix} \sigma_{\Delta\rho}^2 & 0 \\ 0 & \sigma_{\Delta\phi}^2 \end{bmatrix} \quad (10)$$

Incorporating the  $L$  matrix produces the measurement error covariance for  $z$ .

$$R = L\bar{R}L^T \quad (11)$$

Floating values for the integer cycle ambiguities can be estimated using a Kalman filter (Gelb, 1974). The time update is relatively simple due to the relative position and clock bias terms being momentarily removed. The state transition matrix,  $\Phi$ , is an identity matrix, and the process noise matrix,  $Q$ , contains terms along its diagonal.

$$\hat{x}_k = \Phi \hat{x}_{k-1} \quad (12)$$

$$P_k = \Phi P_{k-1} \Phi^T + Q \quad (13)$$

For this work, the diagonal elements of  $Q$  were set to  $0.001\Delta t$ , where  $\Delta t$  is the sample rate of the range measurements. This term could

*Title*

vary depending on the operating environment. For instance, the process noise corresponding to one or all states can be lowered when shadowing or multipath is suspected to reduce the filter's bandwidth and lessen the impact of the degraded signals on the estimate.

The measurement update proceeds based on Equation (9). Although the code based range measurements are noisy relative to the carrier based measurements, they provide an unambiguous measurement and the observability (when four or more satellites are visible) necessary to determine approximate values for the cycle ambiguities. The Kalman filter measurement update is given in Equations (14) through (16).

$$K_k = P_k H_k^T (H_k P_k H_k^T + R)^{-1} \quad (14)$$

$$\hat{x}_k = \hat{x}_k + K_k (z_k - H_k \hat{x}_k) \quad (15)$$

$$P_k = (I - K_k H_k) P_k \quad (16)$$

The integer value of each cycle ambiguity is required to achieve the highest possible accuracy. Double differenced ambiguity estimates must be formed from the single differenced ambiguity estimates to determine an exact integer value (Lawrence, 1996). This vector is formed by choosing a base ambiguity and subtracting all others from it. An  $(m-1) \times m$  matrix ( $C_{DD}$ ) can be formed to perform the operation with 1's along its diagonal and -1's in the column corresponding to the base ambiguity. The double differenced ambiguity and covariance can be expressed as follows:

$$\nabla \Delta \hat{N} = C_{DD} \Delta \hat{N} \quad (17)$$

$$P_{\nabla \Delta \hat{N}} = C_{DD} P_{\Delta \hat{N}} C_{DD}^T \quad (18)$$

An integerization routine is necessary to convert the floating point double differenced ambiguities to fixed point values. The LAMBDA method (de Jonge and Tiberius, 1996) has been proven to provide the highest probability of acquiring the correct set of integer ambiguities among many integer ambiguity acquisition algorithms (Joosten and Tiberius, 2002). It decorrelates the ambiguities to produce a minimized search space and outputs the possible integer solution sets ( $\nabla \Delta \tilde{N}$ ) contained within that space (Joosten, 2001). A common validation technique, known as the ratio test, compares the square norms of the best and second best candidate vectors (Henderson 2001).

Author

$$\frac{(\nabla\Delta\hat{N}_2 - \nabla\Delta\tilde{N})P_{\nabla\Delta\tilde{N}}^{-1}(\nabla\Delta\hat{N}_2 - \nabla\Delta\tilde{N})^T}{(\nabla\Delta\hat{N}_1 - \nabla\Delta\tilde{N})P_{\nabla\Delta\tilde{N}}^{-1}(\nabla\Delta\hat{N}_1 - \nabla\Delta\tilde{N})^T} \geq \kappa \quad (19)$$

If the ratio meets or exceeds a user defined threshold,  $\kappa$ , the first candidate set is deemed valid and used to compute solution.

The carrier phase is used to determine an accurate relative position vector once the ambiguities are known. A double differenced phase observable is formed, and the known ambiguity is removed.

$$\nabla\Delta\phi_{AB}^j = |\Delta\vec{r}_{AB}^j| + \lambda\nabla\Delta\tilde{N}^j + \epsilon_{\nabla\Delta\phi}^j \quad (20)$$

Notice the receiver clock bias term is removed and the noise increases when the double difference operation is performed. The above equation can be rewritten using a double differenced geometry matrix to fit in the form of Equation (9),

$$\nabla\Delta\phi_{AB} - \lambda\nabla\Delta\tilde{N} = C_{DD}G|\Delta\vec{r}_{AB}| + \epsilon_{\nabla\Delta\phi} \quad (21)$$

which can be used in a standard least squares estimation routine to determine a precise relative position.

$$\Delta\vec{r}_{AB} = [(C_{DD}G)^T C_{DD}G]^{-1}(C_{DD}G)^T(\nabla\Delta\phi_{AB} - \lambda\nabla\Delta\tilde{N}) \quad (22)$$

## 2.2. Real Time Performance

The DRTK algorithm was implemented in C++. Two NovAtel PropakV-3 receivers were used to measure range and phase data, which was passed to the DRTK algorithm in order to compute a relative position between two moving vehicles. A Septentrio PolaRx2e receiver was set up at a base station and provided RTK corrections to the NovAtel receivers. The baseline from the base station to the vehicles was logged, and then they were differenced to provide a “true” relative position between the vehicles.

The DRTK solution was logged at 1 Hz for thirty minutes while two vehicles traveled with varying speeds and separation distances. Figure 1 displays the relative North and East error between the DRTK solution and the difference in RTK positions of the vehicles. Note the data was decimated before plotting for clarity purposes. Figure 2 is a

*Title*

histogram containing error information of the magnitude of the relative position vector. Error statistics are given in Table 1.

**Table 1: DRTK error statistics for a 30 minute dynamic test using a differenced RTK solution as truth**

Parameter	Mean	Standard Deviation
$\Delta r_N$	-0.4 mm	3.82 mm
$\Delta r_E$	-0.7 mm	3.1 mm
$ \Delta \vec{r} $	-1.1 mm	3.05 mm

The DRTK solution error seems unrealistically small at first glance. Consider that the DRTK algorithm is similar in principle to a standard RTK algorithm in that a solution is provided once the cycle ambiguities are removed. Therefore, residual errors of the solutions will be correlated. Differencing the solutions removes the correlated portions of the error, yielding optimistic statistics. These statistics imply the true performance of the DRTK solution can be projected to be that of a traditional RTK system, which is 2 cm.

### 3. Vehicle Control

An automated following system using GPS is not as straightforward as one might initially think. An intuitive plan is to follow the lead vehicle's previous position, which is provided by a standalone GPS solution. However, the accuracy of the solution is not high enough to guarantee consistent or safe following accuracy. Using a high quality receiver, one could anticipate a non-differential solution with three meter accuracy which will drift over time and change with satellite geometry. Two receivers in close proximity will experience similar errors, but there is no guarantee they are using the same subset of satellites, and therefore their solutions could be different enough to prevent safe autonomous operation in some scenarios.

#### 3.1. Concept

Given a relative position vector, the angle between two points can be easily calculated in a local East-North-Up (ENU) navigation frame using the relative north and east position ( $\Delta r_N$  and  $\Delta r_E$ , respectively). The relative angle is denoted by  $\psi_R$  and is positive clockwise from North.

$$\psi_R = \text{atan}\left(\frac{\Delta r_E}{\Delta r_N}\right) \quad (23)$$

*Author*

Commanding the following vehicle's heading angle to the relative angle makes the follower point towards the lead vehicle. This creates a towing effect without a physical link between the vehicles. Figure 3 is a schematic demonstrating the concept.

Relative angle accuracy can be expressed as a function of the relative position accuracy and the antenna separation distance.

$$\sigma_{\psi_R} = \text{asin}\left(\frac{\sigma_{\Delta r}}{|\Delta \vec{r}|}\right) \quad (24)$$

A highly accurate relative position is required for short distance following. Figure 4 displays relative angle accuracy versus following distance for three relative positioning accuracies. The DRTK algorithm can provide a suitable reference angle, but a standalone solution will not have sufficient accuracy using this method.

Two deficiencies exist using this method. The following vehicle will not be able to track the lead vehicle path if the lead vehicle performs maneuvers with a turning radius shorter than the baseline length. The constraint of short distance following reduces the possibility of this occurring in many operational environments. The second shortcoming is the inability to replicate the lead vehicle's turning radius, which leads to a lateral path error. The steady state error ( $R_\epsilon$ ) is a function of the lead vehicle turning radius ( $R_L$ ) and the baseline length.

$$R_\epsilon = R_L \left(1 - \sin\left(\arccos\left(\frac{\Delta r}{R_L}\right)\right)\right) \quad (25)$$

Figure 5 is a plot of the error as the turning radius and baseline varies and demonstrates the operational region when using this concept. A short following distance yields low lateral error for most turning radii, and a longer following distance requires larger turning radii to keep the error reasonable.

### *3.2. Controller Design*

A classical proportional-derivative (PD) control law was implemented to drive the error between the following vehicle's heading angle and the relative angle between vehicles to zero. The bicycle model was used to derive the control gains. It is a simple model that captures lateral vehicle dynamics within the linear region of the tire (Gillespie, 1992). The steer angle to yaw rate dynamics are second order, and heading adds an

*Title*

integrator to the system. A non-parametric bicycle model transfer function is expressed as follows:

$$\frac{\psi(s)}{\delta(s)} = \frac{k(s + \tau_z)}{s^3 + 2\zeta\omega_n s^2 + \omega_n^2 s} \quad (26)$$

The pole and zero locations of the bicycle model are functions of both vehicle properties (such as mass, inertia, wheel base, and tire cornering stiffness) and vehicle speed. Therefore, the gains were scheduled with speed to keep the two controllable closed loop poles at a natural frequency of 1 Hz and a damping ratio of 0.707. The uncontrollable pole remained stable throughout the range of operating speeds.

### 3.3. Local Navigation System

A simple kinematic navigation system was written to provide the controller with the necessary information to operate autonomously. Estimated states were speed, longitudinal accelerometer bias, heading, yaw rate gyroscope bias, and North and East position.

$$\hat{x} = [v \quad b_{ax} \quad \psi_F \quad b_{\dot{\psi}_F} \quad N \quad E]^T \quad (27)$$

Inputs to the system were longitudinal acceleration and yaw rate.

$$u = [a_x \quad \dot{\psi}_F]^T \quad (28)$$

The nonlinear kinematic relationships in the navigation model, with white noise driving the bias states, were as follows:

$$\begin{aligned} v_k &= v_{k-1} + \Delta t(a_{x_k} - b_{ax_{k-1}}) \\ b_{ax_k} &= b_{ax_{k-1}} \\ \psi_{F_k} &= \psi_{F_{k-1}} + \Delta t(\dot{\psi}_{F_k} - b_{\dot{\psi}_{k-1}}) \\ b_{\dot{\psi}_k} &= b_{\dot{\psi}_{k-1}} \\ N_k &= N_{k-1} + v_{k-1} \cos(\psi_{F_{k-1}}) \\ E_k &= E_{k-1} + v_{k-1} \sin(\psi_{F_{k-1}}) \end{aligned} \quad (29)$$

GPS measurements were translated to the local ENU frame and provided the estimator with speed, course over ground, and North and East position information.

*Author*

$$z = [v \quad \psi \quad N \quad E]^T \quad (30)$$

Course over ground was used as the heading measurement, which is a valid assumption when the vehicle experiences little to no sideslip under normal operation. Note that course measurement accuracy is inversely related to vehicle speed due to the method by which it is obtained (Daily and Bevly, 2004).

An extended Kalman filter was used to accommodate the nonlinear relationships existing in the model (Gelb, 1974). Execution of the time updated was based on the 20 Hz output rate of the inertial measurement unit (IMU), and the measurement update was performed at 5Hz when GPS measurements were available. The estimator output was a 20 Hz filtered solution of the minimum states required for autonomous operation. However, only the heading estimate was used for this work.

#### **4. Experimental Setup**

Figure 6 shows the vehicles used in the convoy experiment. A Hyundai Santa Fe was the man driven lead vehicle, and an automated ATV Corp Prowler was the following vehicle. Tests were conducted on a closed 1.7 mile oval test course with 300 m diameter, 8 degree banked turns. Throttle was operated manually during the tests as the purpose was to determine the path following capability of the trailing vehicle using the DRTK solution as a reference.

Each vehicle had a NovAtel PropakV-3 GPS receiver to record both raw measurements and an RTK position. A Crossbow IMU440 was mounted on the Prowler and used in its onboard navigation system. Two 900MHz Digi radio modems were used in each vehicle; one received the RTK corrections from a Septentrio PolaRx2e at the base station, and the other transmitted the necessary information between vehicles required by the DRTK algorithm. Each modem pair operated on different channels, and the RTK solution was only used as a measurement of truth for post processed data analysis.

#### **5. Results**

The experimental tests demonstrated the effectiveness of the control strategy outlined in Section 3.1 with the DRTK output used as a reference. The automated Prowler successfully trailed the Santa Fe with following distances ranging from 5 to 50 meters. Behaviour was as anticipated; the Prowler positioned itself as if it were in-tow as it continually oriented its heading to point at the lead vehicle.

*Title*

Deviation from the lead vehicle's path of travel was small, although it was nearly always present. Oscillation with a 5 to 20 second period was present while travelling down the straight sections of the test track. Figure 7 displays the positions of the two vehicles as they travelled along the south portion of the track. Note the scale of the figure due to the slight counter clockwise rotation of the test track. Oscillation is clearly present in the plot and consistent over multiple passes. Figure 8 shows a single pass down the straight section of the track and demonstrates the typical lateral path error. Figure 9 contains the following distance during that pass. The total error over the straight sections had a mean of 5 cm and a standard deviation of 24 cm. The maximum lateral error experienced was 58 cm.

The vehicle acted as expected during the constant radius turns by turning about a smaller radius than the lead vehicle. Oscillations became less persistent in the corners. Steady state path error measured in the turns is listed in Table 2. Interestingly, the path error was smaller than values predicted using Equation (25). This is likely due to an inability to hold the following distance constant. The theoretical path error was derived under the assumption that the centers of rotation for each vehicle were concentric, which is true when the baseline between vehicles is constant. A time rate of change of the baseline invalidates the assumption, and the vehicles rotate about non-concentric points.

**Table 2: Steady state error during constant 150 m radius turns**

<b>Baseline (m)</b>	<b>Actual Error</b>	<b>Theoretical Error</b>
13	0.52	0.56
13.5	0.39	0.61
16	0.72	0.86
17	0.57	0.96

## **6. Conclusion**

A GPS based vehicle platooning system catered towards shorter, LOS following distances was demonstrated. A relative positioning algorithm requiring no installation of temporary or permanent infrastructure was described. A control concept exploiting the accuracy of the relative position measurements was explained, and results from a real time implementation proved the feasibility of the method.

The concept inadequacies were an inability of the following vehicle to track changes in the lead vehicle path that were shorter than the

*Author*

baseline, and a difference in turning radii between the lead and following vehicle. These effects are reduced as the following distance is reduced, and the real time results demonstrated acceptable performance with following distances less than 25 m. Note that some error was due to excessive oscillation which could be addressed with a different control law.

This concept could easily be used in conjunction with an expanded sensor suite containing inertial and perception sensors to provide additional and complementary information. For instance, a laser scanner can be used to determine a range and bearing to the leader, and this can be used in parallel with the DRTK solution or integrated into the DRTK algorithm to improve robustness, especially in areas favorable to GPS signal blockage.

Future work will investigate a more sophisticated control strategy to damp out oscillation and improve tracking performance. Other information will be included as well, such as inertial data and lead vehicle position, pose, and speed data. Finally, methods will be developed to break the LOS constraint and achieve NLOS operation using only GPS and inertial data.

## **References**

- Chen, C., Wang, H., Chew, N., Ibanez-Guzman, J., Jian, S. Wah, C. 'Target Tracking and Path Planning for Vehicle Following in Jungle Environment'. *Proceedings of the IEEE 8<sup>th</sup> International Conference on Control, Automation, Robotics, and Vision. December 6-9, 2004.* Kunming, China.
- Daily, R., Bevely, D.M. (2004) 'The Use of GPS for Vehicle Stability Control Systems', *IEEE Transactions on Industrial Electronics*, Vol. 51, No. 2, pp. 270-277.
- de Jonge, P., Tiberius, C. (1996) 'The LAMBDA Method for Integer Ambiguity Estimation: Implementation Aspects'. Delft Geodetic Computing Centre, Tech. Rep.
- Dogra, S., Wright, J., Hansen, J. (2005) 'Sea-Based JPALS Relative Navigation Algorithm Development', *Proceedings of the 18th International Technical Meeting of the Satellite Division of the Institute of Navigation, September 13-16, 2005.* Long Beach, California.

*Title*

Felter, S. and Wu, N. (1997) 'A Relative Navigation System for Formation Flight'. *IEEE Transactions on Aerospace and Electronic Systems*, Vol. 33, No. 3, pp. 958–967.

Gelb, A., ed. (1974) *Applied Optimal Estimation*, The MIT Press.

Gillespie, T.D. (1992) *Fundamentals of Vehicle Dynamics*, Society of Automotive Engineers, Inc.

Henderson, P.E. (2001) *Development and Testing of a Multiple Filter Approach for Precise DGPS Positioning and Carrier Phase Ambiguity Resolution*. Master's thesis. Air Force Institute of Technology, Wright-Patterson AFB, Ohio.

Hofmann-Wellenhof, B., Lichtenegger, H., Collins, J. (2001) *GPS: Theory and Practice*. Springer-Verlag.

Joosten, P. (2001) 'The LAMBDA-Method: Matlab Implementation', *Mathematical Geodesy and Positioning*, Delft University of Technology, Tech. Rep.

Joosten, P., Tiberius, C. (2002) 'Lambda: Faqs'. *GPS Solutions*, Vol. 6, pp.109–114.

Kaplan, E.D., Hegarty, C.J., eds. (2006) *Understanding GPS: Principles and Applications*. Artech House, Inc.

Kellum, C.C. 'Basic Feasibility of GPS Positioning Without Carrier-Phase Measurements as a Relative Position Sensor Between Two Vehicles', *Proceedings of the 2005 National Technical Meeting of the Institute of Navigation, January 24-26, 2005*. San Diego, California.

Khanafseh, S., Kempny, B., Pervan, B. (2006) 'New Applications of Measurement Redundancy in High Performance Relative Navigation Systems for Aviation', *Proceedings of the 19th International Technical Meeting of the Satellite Division of the Institute of Navigation, September 26-29, 2006*. Ft. Worth, Texas.

Lawrence, D.G. (1996) *Aircraft Landing Using GPS: Development and Evaluation of a Real Time System for Kinematic Positioning Using the*

*Author*

*Global Positioning System*. PhD Thesis. Stanford University, Stanford, California.

Misra, P., Enge, P. (2006) *Global Positioning System: Signals, Measurements, and Performance*. Ganga-Jamuna Press.

Petovello, M., Lachapelle, G., Cannon, M. (2005) 'Using GPS and GPS/INS Systems to Assess Relative Antenna Motion Onboard an Aircraft Carrier for Shipboard Relative GPS', *Proceedings of the 2005 National Technical Meeting of the Institute of Navigation, January 24-26, 2005*. San Diego, California.

Tomizuka, M. (1994) 'Advanced Vehicle Control Systems (AVCS) Research for Automated Highway Systems in California PATH'. *Proceedings of the IEEE Vehicle Navigation and Information Systems Conference. August 31 - September 2, 1994*. Yokohama, Japan.

Travis, W., Bevly, D.M. 'Trajectory Duplication Using Relative Position Information for Automated Ground Vehicle Convoys'. *Proceedings of the 2008 IEEE-ION Position, Location, and Navigation Symposium. May 5-8, 2008*. Monterey, California.

*Title*

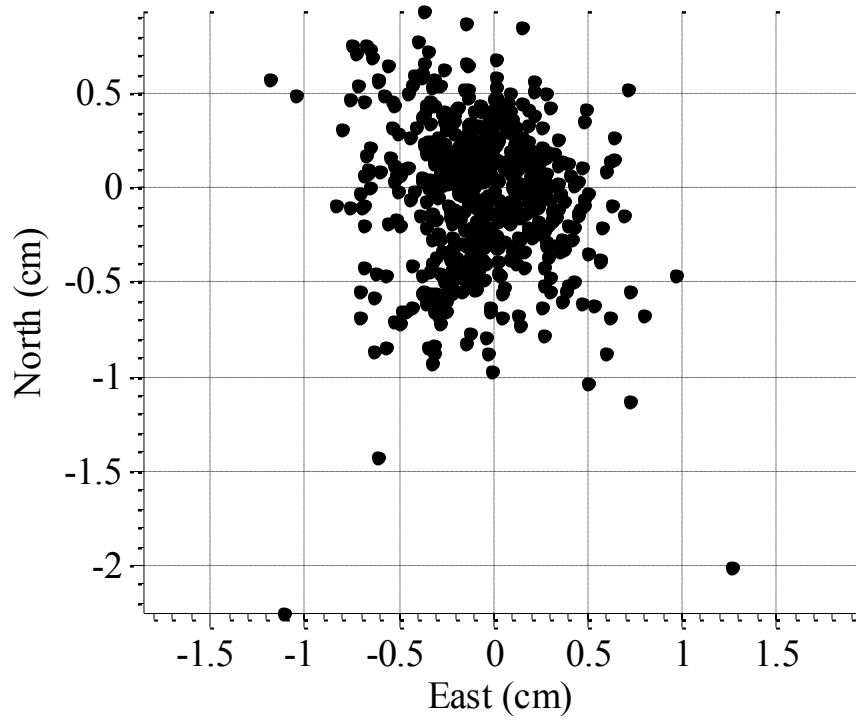


**Figure 1: The scatter plot compares the error between the DRTK relative position and the RTK truth data for a 30 minute dynamic test.**

Author

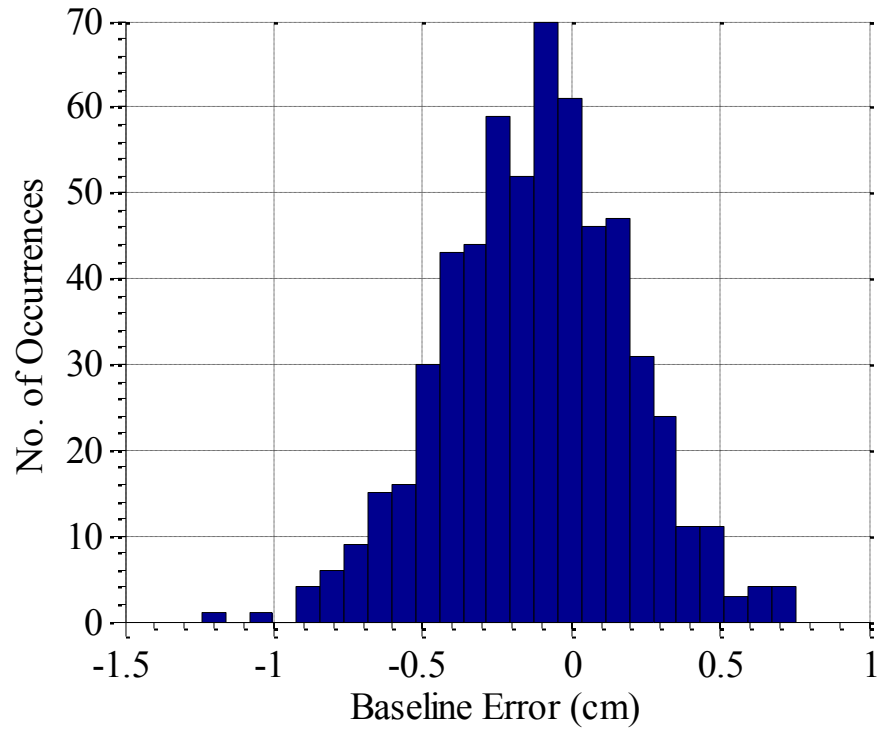
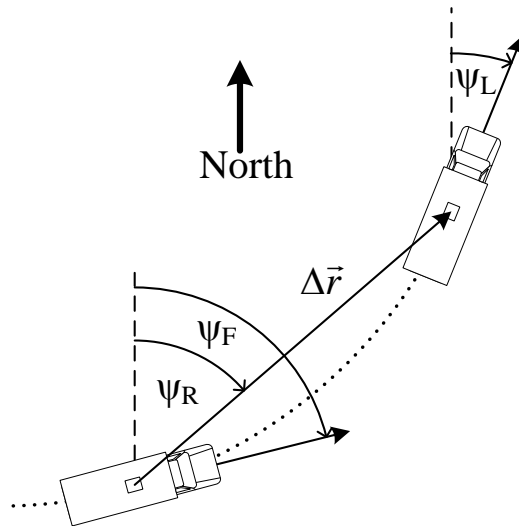


Figure 2: Baseline magnitude error for a 30 minute dynamic test has a mean of -1 mm and a 3 mm standard deviation.

*Title*



**Figure 3: A relative angle between two vehicles can be determined given a relative position vector. The angle can then be used as a control reference to autonomously follow a lead vehicle.**

Author

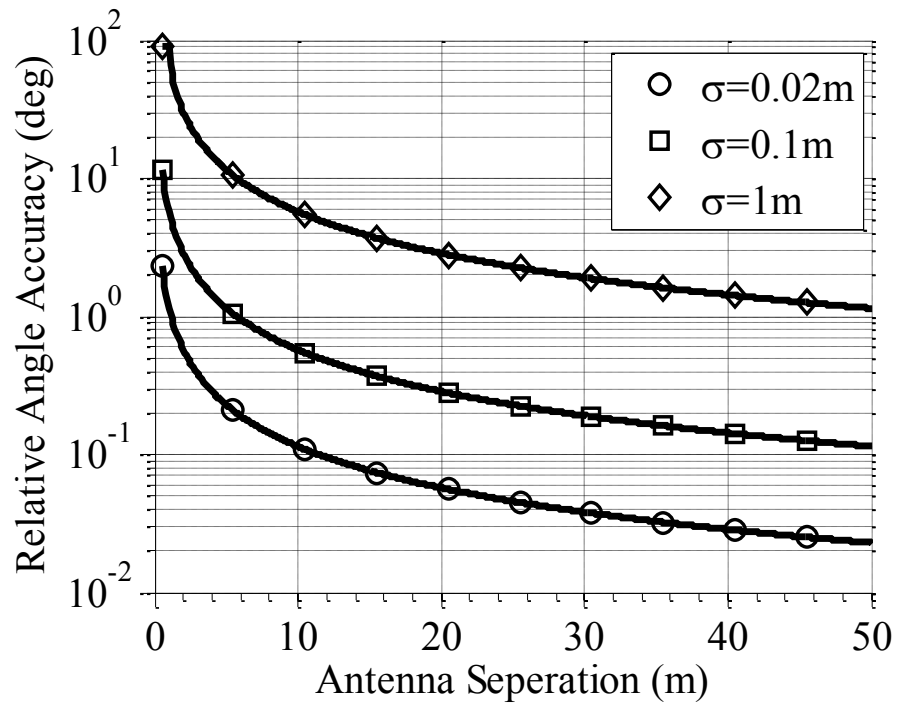
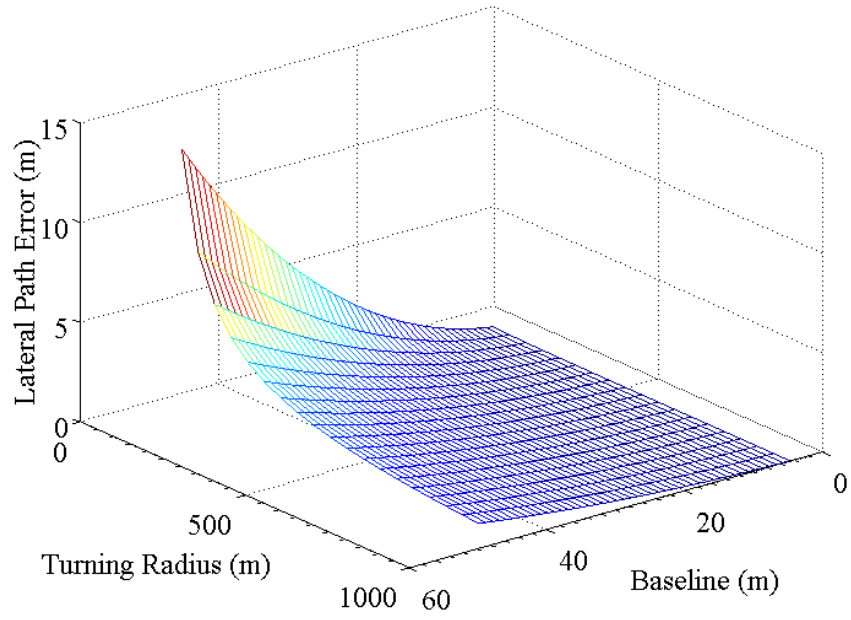


Figure 4: Relative angle accuracy is a function of relative position accuracy and antenna separation distance.

*Title*



**Figure 5: The steady state error is a function of the lead vehicle turning radius and the baseline.**

*Author*

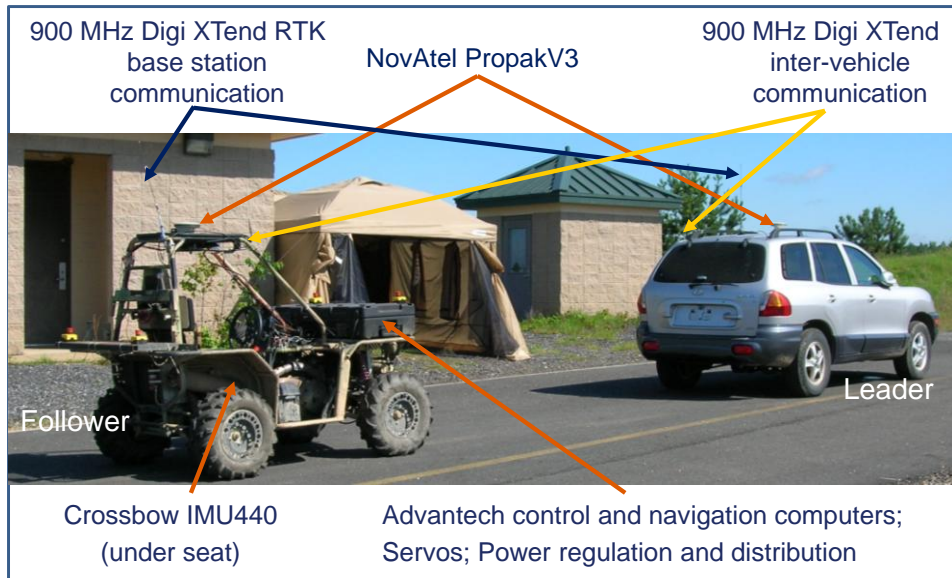


**Figure 6: The tests were conducted with a two vehicle convoy. The Hyundai Santa Fe was man driven, and the ATV Corp. Prowler followed autonomously.**

*Title*

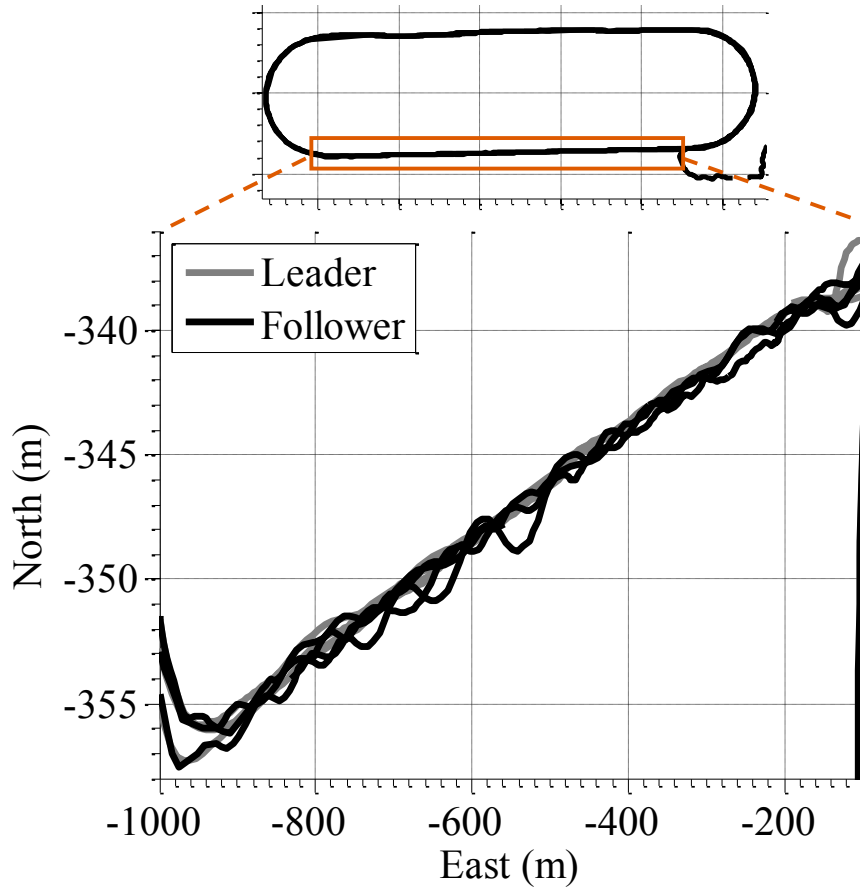


Figure 7: Shown are the positions of the lead and following vehicle (in gray and black, respectively) after multiple passes on the south portion of the track.

*Author*

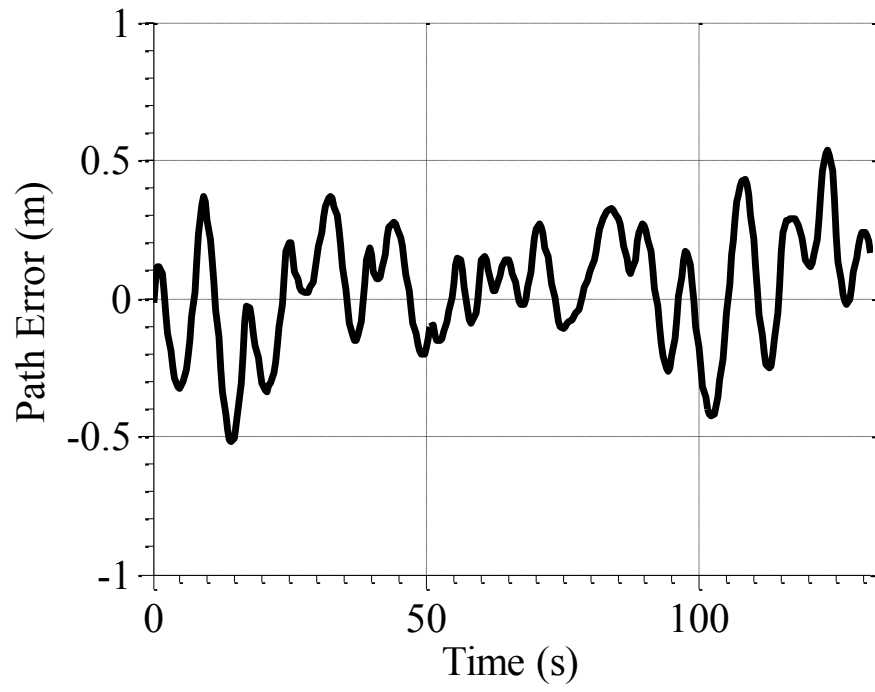


Figure 8: Typical lateral path error while driving straight.

*Title*

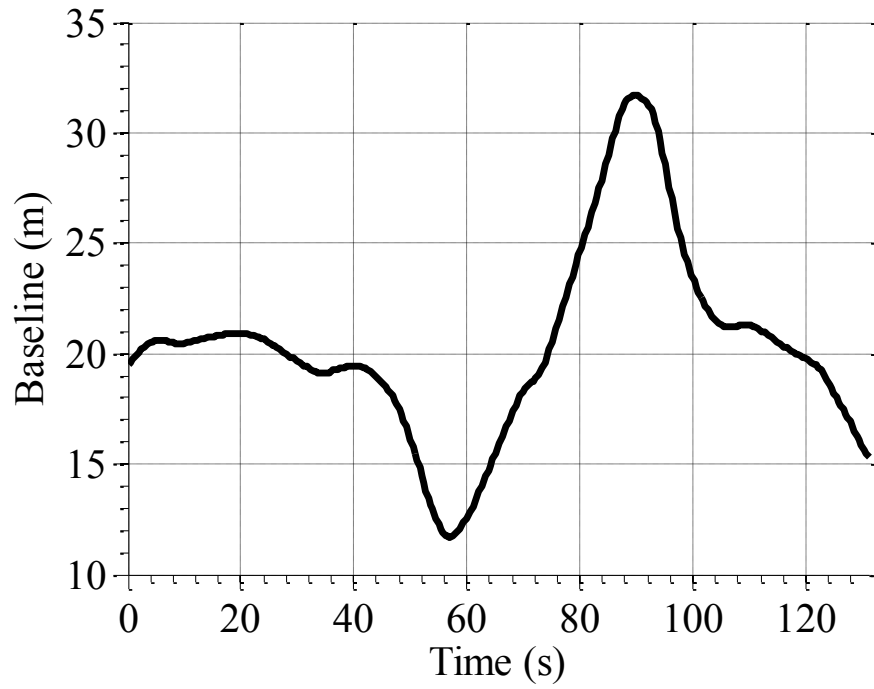


Figure 9: The following distance corresponding to the lateral error in Figure 8.